Effect of cross-field transport on H^- density profile in magnetized plasmas: Comparison between measurement and simulation

Cite as: Phys. Plasmas **14**, 103503 (2007); https://doi.org/10.1063/1.2789559
Submitted: 19 December 2006 . Accepted: 04 September 2007 . Published Online: 16 October 2007

Shin Kajita, Shinichiro Kado, Noriyasu Ohno, Shuichi Takamura, Kiminori Kurihara, and Yosuke Kuwahara

Effect of cross-field transport on H^- density profile in magnetized plasmas: Comparison between measurement and simulation

Shin Kajita[a)]
Graduate School of Engineering, Nagoya University, Nagoya 464-8603, Japan

Shinichiro Kado[b)]
High Temperature Plasma Center, The University of Tokyo, 5-1-5 Kashiwanoha, Kashiwa, Chiba 277-8568, Japan

Noriyasu Ohno
EcoTopia Science Institute, Nagoya University, Nagoya 464-8603, Japan

Shuichi Takamura[c)]
Graduate School of Engineering, Nagoya University, Nagoya 464-8603, Japan

Kiminori Kurihara and Yosuke Kuwahara
Graduate School of Engineering, The University of Tokyo, Bunkyo, Tokyo 113-8656, Japan

(Received 19 December 2006; accepted 4 September 2007; published online 16 October 2007)

The radial density profile of negative hydrogen ions in magnetized plasma is investigated in the divertor simulator MAP (Material and plasma)-II [S. Kado *et al.*, J. Plasma Fusion Res. **71**, 810 (2005)] by measurement and numerical simulation. The laser photodetachment method is used to evaluate the H^- density by considering the influence of the magnetic field. The density of H^- has a hollow profile and exhibits a peak in the peripheral region, though the electron density and temperature exhibit a peak at the center of the plasma column. The density profile of H^- does not agree with the calculation result obtained from the rate equation, in which the local production and extinction rates are balanced, under the present experimental condition. To understand the behavior of negative ions, their trajectories are calculated by numerically solving the equation of motion by considering the effect of collisions. The negative ion density profile calculated from the particle simulation agrees well with the measured negative ion density profile. It is shown that the cross-field H^- transport due to the radial electric field with the assistance of the elastic collisions plays an important role in enhancing the negative ion density in the peripheral region. © *2007 American Institute of Physics*. [DOI: 10.1063/1.2789559]

I. INTRODUCTION

Negative ions can play an important role in various applications such as in negative ion sources for neutral beam injection heating,[2] in the divertor region of experimental fusion reactors,[3] and in plasma processing.[4] For hydrogen negative ions, major production processes are volume production and surface production.[5] It is generally accepted that the dissociative attachment of low-energy electrons to rovibrationally excited hydrogen molecules is the principal volume production process. To effectively produce H^- in ion sources, a magnetic filter[6] is used to separate high-energy electrons from the extraction region of H^-, in which the negative ion density is high. In addition, in order to enhance the surface production of H^-, the vapor of an alkali metal (cesium or sodium) is seeded.[7] The H^- behavior in negative ion sources has been investigated by a numerical simulation and experiments. For the numerical simulation, a numerical code termed NIETZSCHE was developed in the late 1990s.[8] Subsequently, various H^- transport codes have been developed and successfully applied thus far to explain several phenomena in negative ion sources.[9]

In the 1960s, it was reported that there exists a possibility of an increase in the H^- current in the peripheral region of the plasma in a duoplasmatron.[10] From the mid-1980s onwards, linear magnetized plasmas have been used to investigate the possibility of volume production ion sources of H^-.[11–15] The concept of a volume production source without cesium or sodium is particularly attractive because it would avoid the hazardous operation of areas contaminated with the alkali metal vapor. In such studies, negative ions were successfully extracted from the peripheral region by utilizing a Faraday cup; it was demonstrated that two separate regions such as those in the negative ion sources with a magnetic filter were formed in the magnetized plasmas. In other words, rovibrationally excited hydrogen molecules were produced in the central region, and negative ions were produced in the peripheral region, in which the electron temperature was lower than that in the central region. Moreover, in Ref. 15, the effect of the anomalous diffusion on the H^- current has been investigated by changing the radial electric field.

Recently, the behavior of H^- in linear magnetized plasmas has been investigated in similar magnetized devices

[a)]Present address: Japan Atomic Energy Agency, Mukoyama 801-1, Naka, Ibaraki, 311-0193, Japan. Electronic mail: kajita.shin@jaea.go.jp
[b)]Electronic mail: kado@q.t.u-tokyo.ac.jp
[c)]Present address: Aichi Institute of Technology, Yakusa-cho, Toyota 470-0392, Japan.

termed divertor simulators.[16–19] The primary purpose of these studies was to understand the characteristics of the recombination process known as molecular activated recombination (MAR),[3] which is possibly important in the divertor region of nuclear fusion reactors. The density profile and behavior of H^- in the divertor simulators have been investigated by the laser photodetachment (LPD) method, which has been verified to be reliable for measuring the negative ion density locally and absolutely,[20] at least in unmagnetized plasmas.

The H^- density profile in magnetized plasmas has thus far been compared with the calculation results obtained from the rate equation in which the local production and extinction rates are balanced.[16,17,21] However, in the divertor simulator MAP (Material and plasma)-II, the measured H^- density did not agree with the calculation results obtained from the rate equation under certain conditions. It was suspected that the transport effect of H^- is one of the mechanisms for explaining the discrepancy between the experimental and calculation results. Under low-density detached conditions, the negative ions produced in the central region of the plasma column appear to be transported to the peripheral region,[17] whereas under high-density attached conditions, transport loss may occur in the peripheral region.[16] An understanding of the behavior of H^- in linear magnetized plasmas may offer a good insight into the development of linear H^- ion sources and atomic and molecular processes related to MAR. Thus, it is important to investigate the behavior of H^- in magnetized plasmas by considering the transport effect of H^-. Generally, a well-type radial potential profile is formed in magnetized sheet or cylindrical plasmas generated by a dc arc discharge.[22] Since the electric field due to the potential well may force the negative ions to the peripheral region, it is necessary to investigate the transport effect by considering the effect of electric field.

In the present study, the H^- density in the upstream chamber of MAP-II was measured by the LPD method. For the evaluation of the H^- density using the LPD method, the influence of the magnetic field is considered because of the concern regarding whether this method can accurately evaluate the H^- density in magnetized plasmas. Particularly, the influence of the magnetic field was discussed in terms of the collection region of the photodetached electrons (PDEs) and an anomaly occurring in the current-voltage (I-V) characteristics of an electrostatic probe in recombining plasmas. To understand the behavior of the negative ions, we developed a particle simulation code of H^-, in which the transport effect is considered. Based on the comparison between the experimental and simulation results, we showed that the transport of negative ions due to the electric field is a key process for explaining the H^- density profile under the present experimental conditions. The experimental setup and results are provided in Sec. II. In Sec. III, the simulation model and results are presented, and these results are compared with the experimental results. The conclusions are presented in Sec. IV.

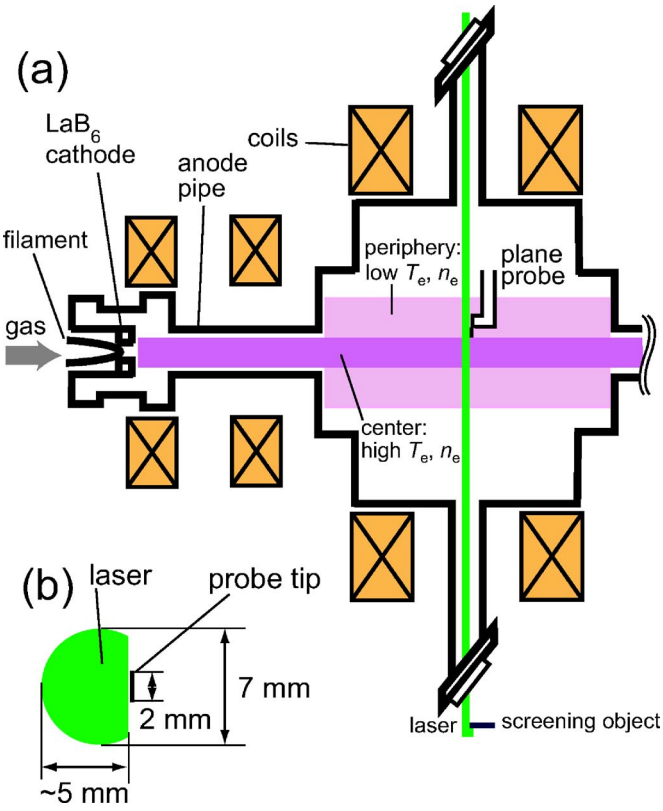

FIG. 1. (Color online) (a) Schematic of the experimental setup in the divertor simulator MAP-II. (b) Schematic of the configuration of probe tip and laser beam channel.

II. EXPERIMENTS

A. Experimental setup

Figure 1 shows the schematic of the experimental setup of the linear discharge device MAP-II.[1] The plasma was generated by a dc arc discharge using a LaB_6 cathode. The magnetic field strength at the center of the plasma chamber was approximately 200 Gauss. Since the radius of the solenoidal coils was sufficiently large, the magnetic field strength at $r=10$ cm decreased by only 2%–3%; the radial dependence of the magnetic field strength was negligible. A cylindrical plasma with a radius and length of several cm and ~2 m, respectively, was formed. Hydrogen was used as the discharge gas, and the neutral pressure at the measurement point was controlled in the range 5.4–33.1 mTorr by injecting additional hydrogen gas into a downstream chamber without utilizing the turbomolecular pump for the upstream chamber. The discharge current and voltage were 45 A and 75 V, respectively. The downstream chamber of MAP-II has thus far been used for investigating the atomic and molecular processes in the divertor region of the fusion experimental reactors in previous studies.[16,17] In the present paper, the negative ion density was measured in the upstream chamber, shown in Fig. 1(a), using pure hydrogen plasmas. Figure 1(b) shows the schematic of the configuration of a probe tip and laser beam channel. A tantalum plane probe with a dimension of 2×2 mm was used for the LPD method. The magnetic field line was normal to the plane probe, and the laser beam was injected parallel to the plane probe, i.e., at an angle of 90° to

the magnetic field line. Typically, the electron Larmor radius is approximately 0.3 mm, which is considerably smaller than the probe tip size; therefore, the experimental configuration corresponds to magnetized regime of electrons. Only one side of the plate was coated with Al_2O_3; therefore, the other side was exposed to the plasmas.[23] When the probe tip surface is damaged by the formation of helium bubbles and holes[24] or contaminated by the impurities such as hydrocarbon, the ablation of the probe surface may lead to the overestimation of the negative ion density in the conventional LPD method.[25,26] In the present study, a screening object (a black-colored object with a dimension of $\sim 2 \times 5$ cm) was placed outside the vacuum chamber, as shown in Fig. 1(a); this resulted in a slab geometry configuration in the eclipse LPD method,[27] in which the laser pulses do not irradiate the probe tip surface directly. When an *in situ* heated probe is used to clean the probe surface, ablation occurs less frequently, and in the case of pure hydrogen plasmas, the threshold pulse energy of the ablation becomes several hundred mJ/cm^2.[26]

When the LPD method is used to measure the negative ion density in magnetized plasmas, particularly in low-temperature recombining plasmas, several problems have to be dealt with. The first problem regarding the collection region of the probe is that in magnetized plasmas, this region may elongate along the magnetic field line. For the LPD method, the collection region of the PDEs,[28] which corresponds to the minimum necessary laser beam size for accurately measuring n_-,[29] is a matter of concern. The negative ion density is underestimated unless the laser beam size is sufficiently large, typically several mm in radius in unmagnetized plasmas.[29] The behavior of the collection region of the PDEs in magnetized plasmas has also been investigated.[30] In Ref. 30, it has been verified that the collection region of the PDEs depends neither on the strength of the magnetic field nor on the probe tip size under experimental conditions similar to those in the present study. The length of the laser beam used in the experiments was 5 mm along the magnetic field, as shown in Fig. 1(b); therefore, the laser beam was sufficiently large as compared to the collection region of the PDEs.

The second problem to be dealt with is the reduction in the electron current due to the magnetic field. In particular, in low-temperature recombining plasmas, it has been reported that the I-V characteristics of a single probe become similar to those of a double probe. Therefore, the absolute value of the electron current may not be used for the measurement. A detailed discussion regarding the effect is provided later with the experimental results.

B. Experimental results

Figure 2(a) shows the radial profile of the electron density n_e and temperature T_e measured with the electrostatic probe. The neutral gas pressure was 5.4 mTorr. In strongly magnetized plasmas, it is common to use only the net ion-collecting part of the I-V characteristics to determine T_e and n_e.[33] In the present analysis, we used only the net ion-collecting part; however, anomalous I-V characteristics in

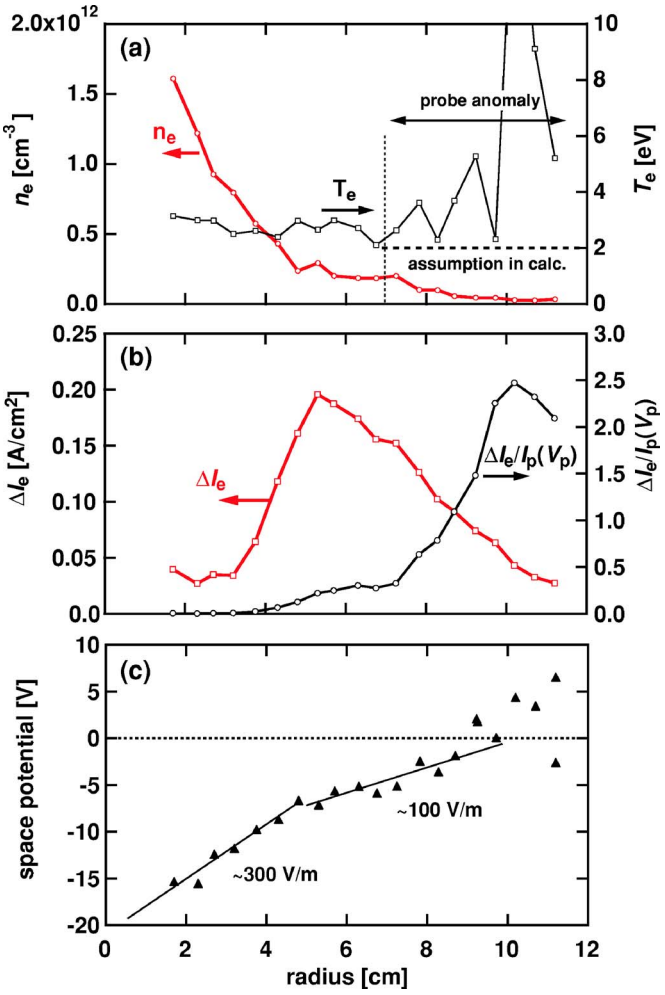

FIG. 2. (Color online) Radial profiles of (a) electron density and temperature, (b) ΔI_e and $\Delta I_e/I_p(V_p)$, and (c) space potential. The pressure of neutral hydrogen is 5.4 mTorr (Shots Nos. 25148–25164).

the recombining plasma led to the overestimation of the electron temperature in the peripheral region of the plasma column in a manner similar to that in previous studies in a tokamak[34] and divertor simulators.[31,35] Therefore, we assumed that the electron temperature at $r > 7$ cm was 2 eV. Figures 3(a) and 3(b) show the probe I-V characteristics at $r = 2$ cm and 9 cm, respectively. It was observed that the electron current of the probe is reduced drastically at $r = 9$ cm, and the I-V characteristics were similar to those of the double probe. Figure 3(c) shows the ratio of the probe current at the space potential to the ion current, i.e., $I_p(V_s)/I_i$, as a function of r. When we evaluate I_i from the probe characteristics, its value at the space potential, which is extrapolated from the negatively biased part of the I-V characteristics, is used for eliminating the expansion effects of the probe collection area. Without the anomalous reduction in the probe current, $I_p(V_s)$ and I_i are written as follows:

$$I_p(V_s) \simeq \tfrac{1}{4} e n_e v_{e,\mathrm{th}} S, \tag{1}$$

$$I_i = \kappa e n_e C_s S, \tag{2}$$

where e is the elementary charge, S is the surface area of the probe tip, m_e and m_i are the electron and ion mass, respec-

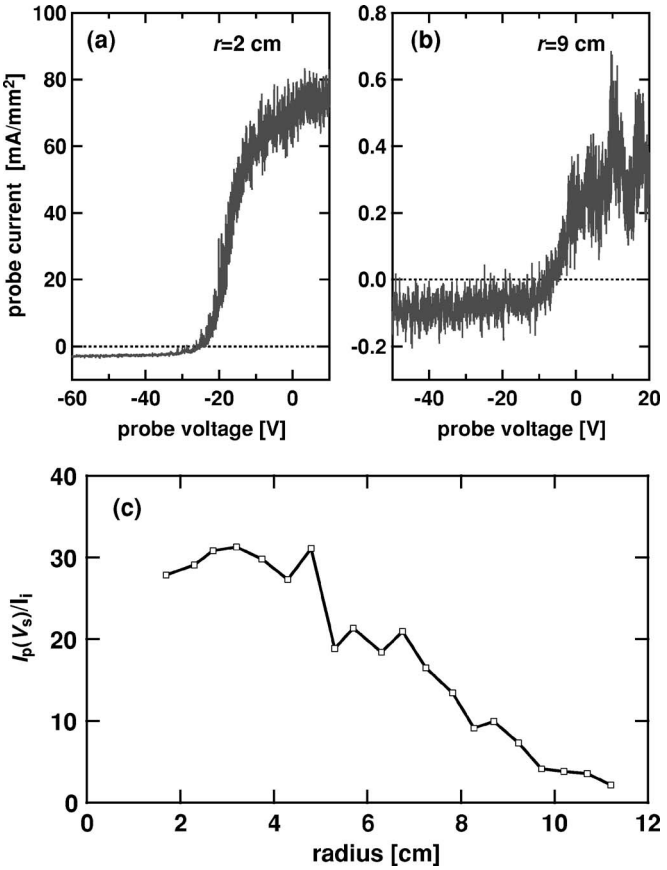

FIG. 3. Probe current-voltage characteristics at (a) $r=2$ cm and (b) 9 cm and (c) radial profile of the ratio of electron current to ion current $I_p(V_s)/I_i$ at space potential.

tively, and κ is a constant whose value is 0.61 for $T_i \ll T_e$. $v_{e,\mathrm{th}}$ is the thermal velocity of the electrons defined as $\sqrt{8kT_e/\pi m_e}$, and we use $C_s=\sqrt{kT_e/m_i}$ for the ion sound velocity under the assumption that $T_i \ll T_e$. Only the contribution of the electrons is considered for $I_p(V_s)$ in Eq. (1). From Eqs. (1) and (2), the ratio $I_p(V_s)/I_i$ becomes

$$\frac{I_p(V_s)}{I_i} \simeq \frac{1}{\kappa}\sqrt{\frac{1}{2\pi}\frac{m_\mathrm{i}}{m_\mathrm{e}}}. \tag{3}$$

In Fig. 3(c), the ratio drastically decreases with r, though $I_p(V_s)/I_i \sim 30$, which corresponds to the value estimated from Eq. (3), around the column center.

If the negative ion ratio increases, it is necessary to consider the effect of the negative ions in Eq. (3). According to Refs. 36 and 37, due to the contribution of the negative ions, the ratio $I_p(V_s)/I_i$ changes as follows:

$$\frac{I_p(V_s)}{I_i} = \frac{\sqrt{m_i/2\pi m_e}+(n_-/n_e)\sqrt{1/2\pi\gamma}-(1+n_-/n_e)\sqrt{1/2\pi\gamma}}{(\exp(-\eta)+(n_-/n_e)\exp(-\gamma\eta))\sqrt{2\eta}}, \tag{4}$$

where γ is the ratio of the electron temperature to the negative ion temperature, and

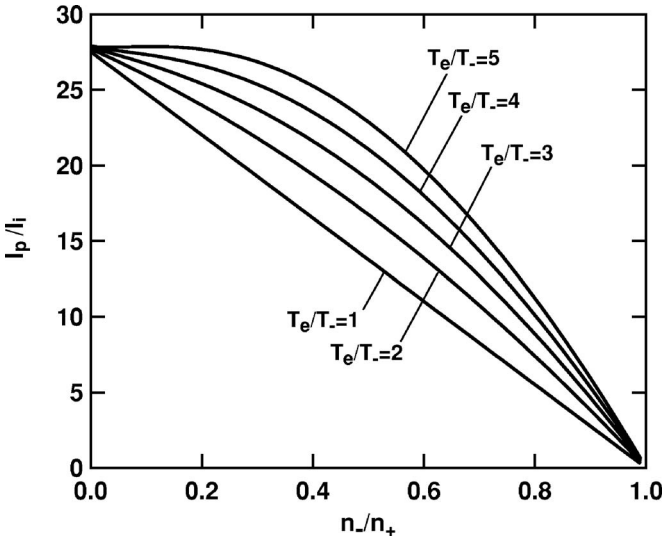

FIG. 4. Ratio $I_p(V_s)/I_i$ vs n_-/n_+ for different T_e/T_i.

$$\eta = 0.5\frac{1+n_-/n_e}{1+\gamma(n_-/n_e)}. \tag{5}$$

For simplicity, it is assumed that the positive and negative ion temperatures are the same and the positive and negative ions have the same mass in Eq. (4). Figure 4 shows the ratio $I_p(V_s)/I_i$ calculated from Eq. (4) versus n_-/n_+ for different values of T_e/T_i. The ratio $I_p(V_s)/I_i$ decreases linearly with n_-/n_+ when $T_e/T_-=1$. When $T_e/T_- > 1$, $I_p(V_s)/I_i$ decreased to a moderate extent.

Under the present experimental conditions, it is unlikely that $T_e/T_- < 1$; therefore, the reduction in $I_p(V_s)/I_i$ in the peripheral region, as shown in Fig. 3(c), indicates that $n_-/n_+ \gtrsim 0.9$, i.e., $n_-/n_e \gtrsim 9$ if $I_p(V_s)/I_i$ is reduced only due to the negative ions. Figure 2(b) shows the radial profiles of ΔI_e and $\Delta I_e/I_p(V_p)$, where ΔI_e is the excess electron current in response to the laser pulse and $I_e(V_p)$ is the probe current (electron current) measured along with ΔI_e using the positively biased probe. In contrast to the profile of n_e whose peak is at the center, the peak of ΔI_e is located at $r \sim 5$ cm. It can be observed that the maximum value of $\Delta I_e/I_p(V_p)$ is 2.5, which is considerably lower than the ratio n_-/n_e equal to 9 obtained from Eq. (4) in the peripheral region. This indicates that the reduction in $I_p(V_s)/I_i$ is caused by factors other than the effect of the negative ions.

In certain cases, it has been reported that the electron current of the probe reduces drastically. The anomaly in the single-probe characteristics has been widely reported in a tokamak[34] and divertor simulators.[31] Moreover, in divertor simulators, such an anomaly has been observed not only in hydrogen plasmas[35] but also pure helium plasmas,[31] in which negative ions do not exist. Although the physical mechanism of the anomalous I-V characteristics is not yet entirely clear, the mechanism is considered to be the plasma impedance between a probe tip and a reference electrode and/or by fluctuating space potential.[32] Similarly, in the present study, it is believed that the electron current was reduced due to the probe anomaly in the peripheral region; therefore, it is better

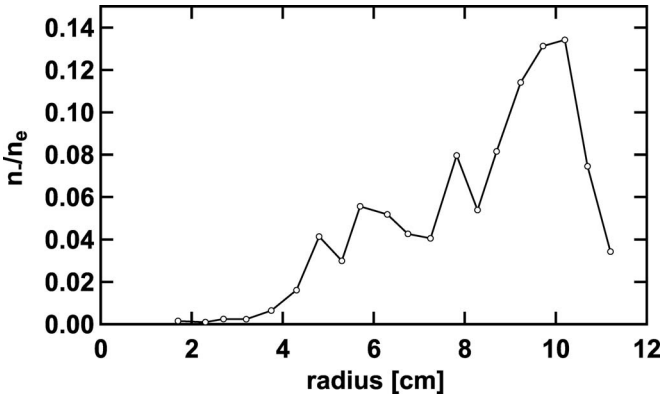

FIG. 5. Radial profile of n_-/n_e evaluated from Eq. (10).

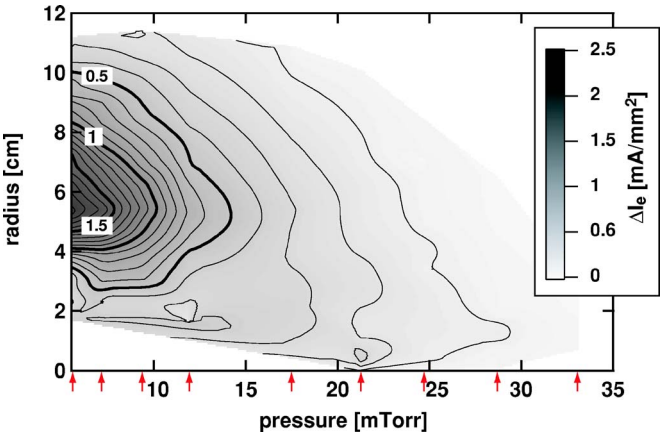

FIG. 6. (Color online) Contour plots of ΔI_e as functions of neutral pressure and radial distance. The measurements were performed at 5.4, 7.2, 9.4, 12.0, 17.5, 21.3, 24.8, 28.7, and 33.1 mTorr (Shots Nos. 25148–25270).

to rely on the positive ion current, which is considered to be more accurate in recombining plasmas, as shown in Ref. 32.

Usually, the following equation is used to evaluate the negative ion density when the laser pulse energy is sufficiently high to saturate the photodetachment signals,[20,38]

$$\frac{\Delta I_e}{I_p(V_p)} = \frac{n_-}{n_e}\sqrt{\frac{T_{\text{eff}}}{T_e}}, \tag{6}$$

where T_{eff} is the effective temperature of the excess electrons collected by the probe. The term $\sqrt{T_{\text{eff}}/T_e}$ represents the difference between the energies of the PDEs and bulk electrons. While investigating T_{eff}, we should consider the thermalization process and particle exchange process of the PDEs. The time required for the thermalization of the PDEs can be written as[2]

$$\tau = \frac{3\sqrt{2}\pi^{3/2}\epsilon_0^2 m_e^{1/2}}{n_e e^4 \ln\Lambda}(T_e + T_{\text{PDE}})^{3/2}, \tag{7}$$

where T_{PDE} is the effective initial temperature of the PDEs. Given that $\ln\Lambda = 10$ and $T_{\text{PDE}} \sim T_e \sim 2$ eV, τ becomes $\sim$50 ns for $n_e = 10^{12}$ cm^{-3} and 500 ns for $n_e = 10^{11}$ cm^{-3}. Thus, the thermalization time of the PDEs in the peripheral region is longer than the rise time of the LPD signal ($\sim$50 ns). With regard to the particle exchange process of the PDEs, detailed numerical[40] and experimental[39] investigations have been reported. In Ref. 39, it has been experimentally shown that the energy of the PDEs does not depend on the photon energy, although the thermalization time of the PDEs is longer than the rise time of the LPD signal. This behavior has been attributed to the exchange process of the PDEs and bulk electrons. We experimentally identified that T_{eff} obtained from the probe voltage dependence of ΔI_e is almost the same as $I_e(V_p)$ in MAP-II. This may be attributed to the fact that $T_{\text{PDE}} \sim 1.6$ eV (photon energy of 2.33 eV; electron affinity of 0.75 eV) can be approximated to $T_e \sim 2$ eV in the peripheral region of MAP-II in addition to the particle exchange and thermalization processes of the PDEs. Therefore, we adopted the assumption of $T_{\text{eff}} \sim T_e$ in this study.

From Eq. (1), n_e is written as

$$n_e = \frac{4I_{e0}}{ev_{e,\text{th}}S}. \tag{8}$$

By substituting Eq. (8) in Eq. (6), the negative ion density is[17]

$$n_- = \frac{\Delta I_e}{eS}\frac{I_p(V_s)}{I_p(V_p)}\frac{4}{\sqrt{8kT_{\text{eff}}/\pi m_i}}. \tag{9}$$

Even if the value of the electron current $I_p(V_s)$ is affected by the probe anomaly and Eq. (8) cannot be used to determine n_e, only the relative value of the electron current $I_p(V_s)/I_p(V_p)$ is used in Eq. (9). Thus, we can obtain an accurate n_- from Eq. (9) even when a probe anomaly occurs. Using Eqs. (2) and (9), n_-/n_e can be written as follows, instead of Eq. (6):

$$\frac{n_-}{n_e} = \frac{\kappa\Delta I_e}{I_i}\frac{I_p(V_s)}{I_p(V_p)}\sqrt{\frac{\pi}{2}\frac{m_e T_e}{m_i T_{\text{eff}}}} \sim \frac{\kappa\Delta I_e}{I_i}\frac{I_p(V_s)}{I_p(V_p)}\sqrt{\frac{\pi}{2}\frac{m_e}{m_i}}. \tag{10}$$

Then, the negative ion density ratio can be determined even when an anomaly occurs in the electron current in the recombining plasmas. The important points to be considered while evaluating the negative ion density ratio by Eq. (10) are the use of the ion current and the relative value of the electron current in stead of the use of the absolute value of the electron current.

Figure 5 shows the radial profile of n_-/n_e evaluated from Eq. (10). By using the ion current, the influence of the anomalous reduction in the electron current was modified; the maximum negative ion density ratio n_-/n_e was evaluated to be 15%. It was observed that n_-/n_e was overestimated when Eq. (6) was used under the present experimental conditions because of the anomalous reduction in the electron current in the peripheral region. Figure 2(c) shows the radial profile of the space potential measured by the electrostatic probe. A potential well with a depth of approximately −20 V was formed at the center of the plasma column.

Figure 6 shows the contour plots of ΔI_e as the functions of the radial distance and hydrogen gas pressure. Since the

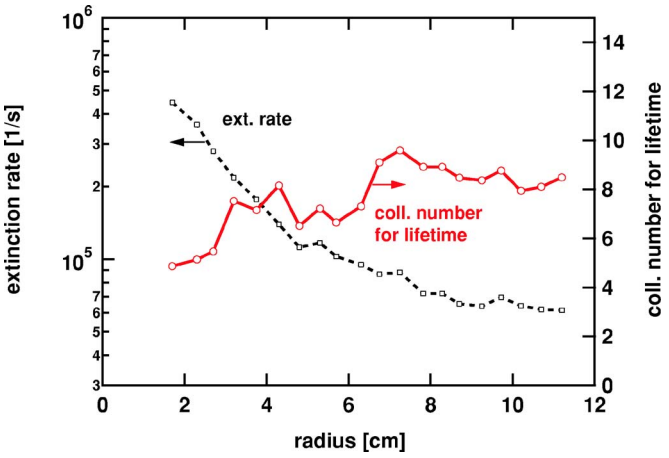

FIG. 7. (Color online) Radial profiles of extinction rate of H^- and number of elastic collisions with H_2 and H^+ within the lifetime.

probe anomaly occurred even in the central region of high neutral gas pressure regimes, ΔI_e was plotted in Fig. 6 instead of n_e. As the gas pressure increased, the peak position of ΔI_e shifted closer to the central region. One reason for this shift is that T_e decreases with an increase in the gas pressure. The transport effect may also influence the profile of H^-. In the present study, we desire to focus on the H^- density profile under the lowest pressure condition of 5.4 mTorr; the variation in the transport effect due to the increase in the gas pressure can be investigated in a future work.

Before discussing the transport effect in detail in the next section using a simulation method, the possibility that this effect causes a change in the H^- profile is mentioned in this paper following our previous qualitative discussions in Sec. 4.2 of Ref. 1. Figure 7 shows the radial profiles of the calculated extinction rate of the negative ions and the number of the elastic collisions within their lifetime. The extinction processes considered here are the electron detachment processes by the collisions with e^- and H, and mutual neutralization. The density profile of H was assumed to be uniform, and the degree of dissociation of H_2 was assumed to be 5%. With regard to the elastic collision processes, the collisions with hydrogen molecules and with positive ions[41] were considered with the assumption that $T_i=T_e/5$. The extinction rate decreased with r because of the decrease in n_e and T_e. In the peripheral region, the collision with H is the principal extinction process as compared to the collisions with electrons and ions; therefore, the extinction rate becomes rather flat at $r>8$ cm. With regard to the elastic collision, Coulomb collision with positive ions is dominant around the center, while the collision with the hydrogen molecules is dominant in the peripheral region. At $r\sim 2$ cm, the number of collisions was approximately five, even though the lifetime was approximately 2 μs because of the high electron/ion density. On the other hand, the number of collisions for the negative ions produced in the peripheral region would be ten during ~ 10 μs. Assuming that the radial velocity of H^- is ~ 10 km/s, which is the typical H^- velocity in MAP-II,[23] the distance traveled within the entire lifetime would be from ~ 2 cm (at $r=2$ cm) to 20 cm (at $r=10$ cm). Although the cross-field effect was not considered in the assumption of the radial velocity of H^-, the simulation results shown later indicate that the assumption does not contradict the actual situation. It may be difficult for the negative ions to escape from the central region because the distance to be traveled is short; it is possible that the negative ions produced between the center and the peripheral region (for example, $3<r<5$ cm) contribute to enhancing the density in the peripheral region (for example, $5<r<10$ cm) due to a sufficient number of elastic collisions.

III. SIMULATION

A. Simulation model

In order to investigate the effect of the cross-field transport of H^-, the trajectories of the negative ions were calculated by numerically solving the equation of motion with two dimensions x and y and three velocities v_x, v_y, and v_z as follows:

$$m_- \frac{d\boldsymbol{v}}{dt} = -e(\boldsymbol{E} + \boldsymbol{v} \times \boldsymbol{B}) + \boldsymbol{F}_{\mathrm{coll}}, \tag{11}$$

where m_- is the mass of H^- in kg, $\boldsymbol{v}$ is the velocity of H^- in m/s, e is the elementary charge in C, $\boldsymbol{E}$ is the electric field vector in V/m, $\boldsymbol{B}$ is the magnetic field vector in T, and $\boldsymbol{F}_{\mathrm{coll}}$ is the collision term. The following three extinction processes of H^- and the elastic collision with neutral particles are considered by using the Monte Carlo method in each time step: (1) collision with electrons, $H^- + e \rightarrow H + 2e$, (2) mutual neutralization, $H^- + H^+ \rightarrow 2H$, and (3) collision with H, $H^- + H \rightarrow H_2 + e$ and $H^- + H \rightarrow 2H + e$. In addition to these collisional processes, Coulomb collisions with electrons and positive ions are considered.[42,43] The extinction process due to the collision with H_2 is neglected because the extinction rate is substantially lower than that of the collision with H.[44,45] The extinction due to the collision with the chamber wall, which occurs due to the effect of the parallel transport, is considered in each time step by the Monte Carlo method. The extinction probability due to the parallel transport can be determined from the ratio of the negative ion flux toward the wall to the total negative ions. If all the particles are produced at the center of the chamber, the transport is determined from the diffusive process; therefore, $\tau \sim L_{\mathrm{cham}}^2/D_{\parallel}$. In the diffusion model, the parallel transport time is of the order of 1 ms, which is significantly longer than the extinction time due to the collision process. However, in actual situations, the production of the negative ions in the parallel direction is almost uniform because the gradients of the electron temperature and density are small. Therefore, we should precisely evaluate the parallel H^- density profile in order to estimate the H^- flux toward the wall. For simplicity, we assumed that the negative ion density in the parallel direction is constant and the flux toward both the walls is $\sim n_- v_z$ per unit area. This corresponds to the regime termed "sheath limited regime." The use of the transport time of $\sim v_z \Delta t / L_{\mathrm{cham}}$ creates an ambiguity and it may slightly overestimate the parallel transport effect; however, this does not cause a critical problem under the present experimental conditions because the extinction due to the collisions with electrons, positive ions and H are

the principal extinction processes. We used a simplified model in this study; the parallel H^- density profile can be investigated in a future work by measurement and simulation.

Negative ions were generated at random in the x-y space by applying their calculated production rate. The initial kinetic energy of the generated negative ions is assumed to be 0.3 eV based on the calculation by Wadehra,[46] in which the initial kinetic energy of the negative ions produced by the dissociative attachment of H_2 is estimated to be in the range 0.2–0.4 eV. The time step size in the simulation was 10 ns, which is sufficiently shorter than the time scale of the cyclotron motion of H^-.

Figure 8(a) shows the trajectories of the negative ions without collisional effects. The trajectory is circular and its guiding center moves in the $\boldsymbol{E}\times\boldsymbol{B}$ direction. Thus, it is difficult to enhance the negative ion flux toward the radially outer region when collisions do not occur, although the negative ions move cyclically in the radially outer and inner directions. Figure 8(b) shows the typical calculated trajectories of the negative ions. The calculations were continued until the particle disappeared due to the extinction processes by collisions and parallel transport; the trajectories of some particles are extremely short, while those of others are rather long. Let us consider the trajectories of particles marked as (a), (b), and (c). All the particles gradually move toward radially outer region as moving in the direction of $\boldsymbol{E}\times\boldsymbol{B}$. Particle (a) was produced at r=6.1 cm and destroyed at r =14.4 cm after 13.2 μs, particle (b) was produced at r =4.1 cm and destroyed at r=8.8 cm after 5.6 μs, and particle (c) was produced at r=4.0 cm and destroyed at r =5.9 cm after 1.4 μs. The averaged radial speeds of particles (a), (b), and (c) were 6.3, 8.4, and 13.6 km/s, respectively. The velocities do not contradict the assumption of radial speed of H^- used in Sec. II.

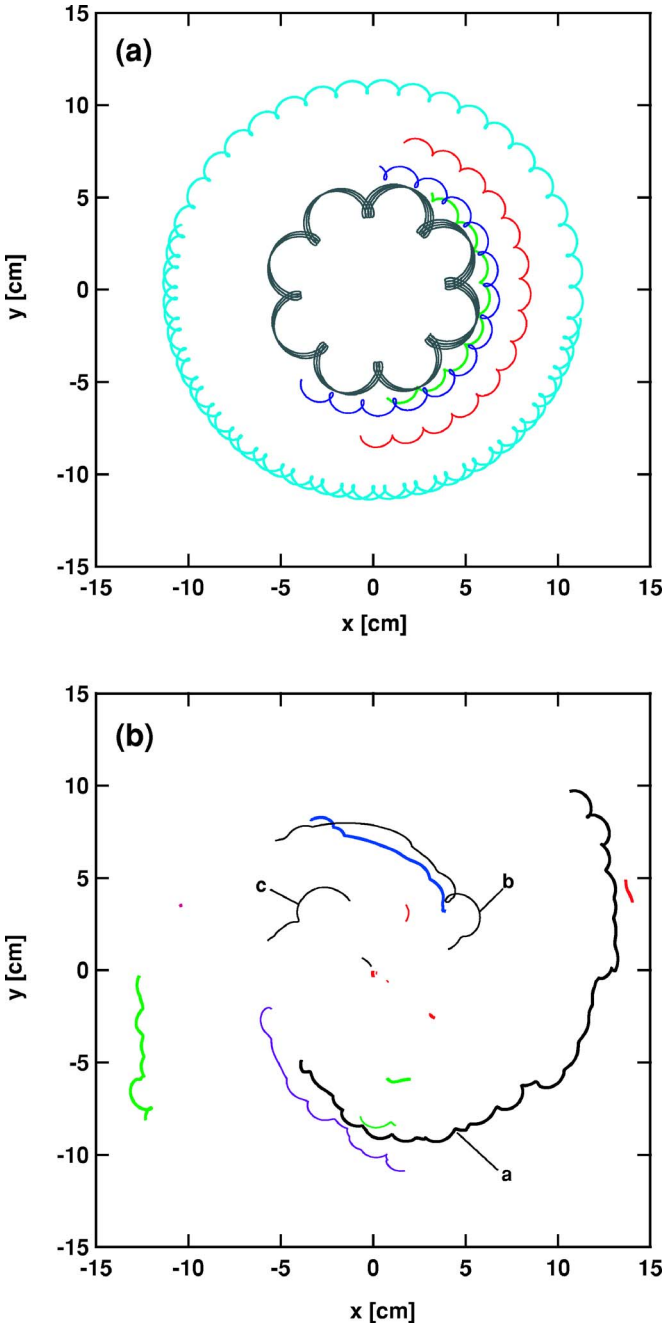

FIG. 8. (Color online) Typical calculated trajectories of negative ions (a) without collisions and (b) with collisions.

B. Simulation results and discussion

The negative ion density without considering the cross-field transport is obtained from the steady state solution of the rate equation including the major production and extinction processes. The negative ion density is evaluated as follows:

$$n_- = \sum_{0\le v\le 9} \frac{n_e \alpha_{e,H_2} n_{H_2(v)}}{n_e \alpha_{e,H^-} + n_{H^+}\alpha_{H^+,H^-} + n_H \alpha_{H,H^-} + 1/\tau}, \qquad (12)$$

where α_{e,H_2}, α_{H^+,H^-}, α_{e,H^-} and α_{H,H^-} are the rate coefficients for dissociative attachment, mutual neutralization, electron detachment due to the collision with electrons, and electron detachment due to the collision with H, respectively; n_H is the density of atomic hydrogen, and $1/\tau$ represents the extinction due to the parallel transport. Figure 9(b) shows the comparison of the calculated and measured H^- density profiles. Case (i) in Fig. 9(b) shows the H^- density obtained from Eq. (12) by applying T_{vib}=5000 K and $\tau = L_{cham}/C_s$, where C_s is the ion sound velocity under the assumption that the parallel H^- velocity is equivalent to the ion sound velocity. This assumption does not imply that H^- is accelerated by presheath as positive ions. It was based on the previous measurement of the H^- velocity in MAP-II,[23] in which the speed of H^- was comparable to the ion sound speed.

The calculation based on the rate equation yields a lower H^- density in the peripheral region as compared to the H^- density obtained from the experiments; the H^- density profile exhibiting a peak at approximately 5 cm cannot be reproduced. It is observed that in the calculation based on the rate equation, the spatial profiles of the vibrational temperature and H density are assumed to be constant. In MAP-II, the vibrational temperature and the degree of dissociation have been measured using passive spectroscopy.[17,47] The gas pressure dependence of the vibrational population distribution obtained by detailed modeling is different from the gas pres-

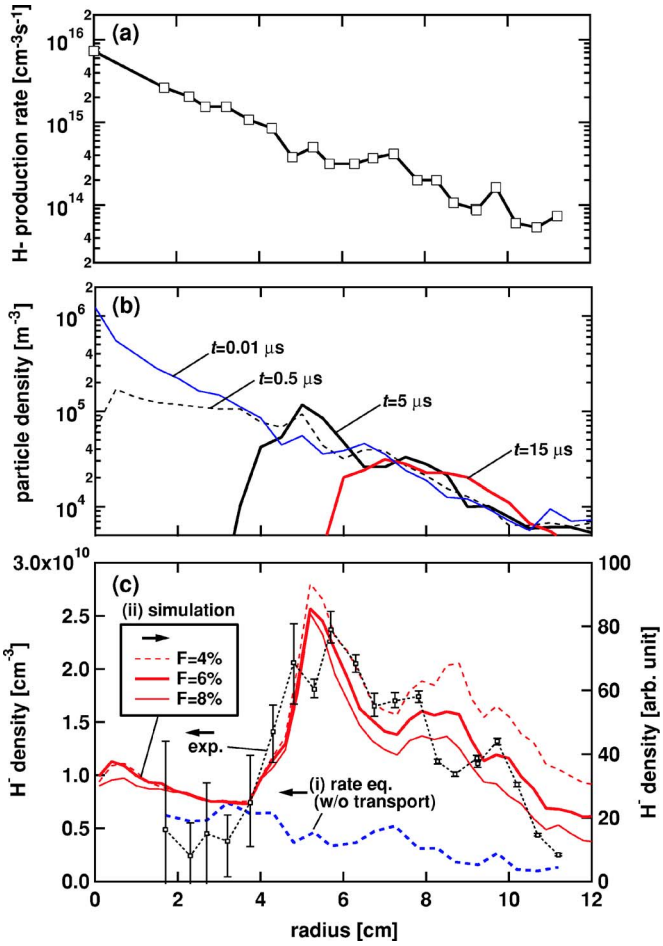

FIG. 9. (Color online) (a) Radial profile of production rate of H^-, (b) evolution of density profile of test H^- particles produced at $t=0$, and (c) comparison between calculated and measured H^- density profiles. Cases (i) and (ii) represent the calculation results from Eq. (12) and particle simulation, respectively.

sure dependence in the current experiments.[48] Regarding the profile of H, since the degree of dissociation is low (several %) and the lifetime of H is reasonably long, i.e., roughly $\lesssim$0.1 ms even around the plasma center due to a low reaction rate of ionization (typically lower than 10^{-9} cm^3/s), it is likely that the H density profile is determined mainly by the diffusion process and the loss due to the collision with the chamber wall. Qualitatively, if the H density decreases with the radius, the H^- density profile obtained from the simulation may extend to the peripheral region; whereas, the H^- density in the peripheral region may decrease if the vibrational temperature in the peripheral region is lower than that in the central region. However, a spatial profile cannot be obtained by passive spectroscopy; therefore, these effects can be investigated in a future work by the use of other precise measurements such as laser-induced fluorescence. Then, in this study, we focus on the transport effects of H^- by a simulation.

Figure 9(a) shows the radial profile of the production rate of H^- from the dissociative attachment of $H_2(v)$, which corresponds to the numerator on the right-hand side of Eq. (12). The production rate in the central region was estimated by extrapolating T_e and n_e around this region. The production profile of the test H^- particles in the simulation was weighted by this production rate. Figure 9(b) shows the evolution of particle number density by using 5000 test H^- particles produced at $t=0$. The radial mesh size for evaluating the particle density in Fig. 9(b) was 5 mm. Under the present experimental conditions, the negative ions produced in the chamber were calculated to be of the order of 5×10^{19} s^{-1}. By considering the time step size of 10 ns and 5000 test particles, the weight of one test particle is evaluated to be of the order of 10^8. At $t=0.01$ μs, the particle distribution indicates the production distribution of the negative ions. Since the production rate is proportional to the electron density, the production distribution exhibits a peak at the center. However, the negative ions around the central region disappeared rapidly in several μs because the extinction rate was high due to higher electron density and temperature in the central region; in addition, the particles were transported to the peripheral region due to the electric field. After 5 μs, the negative ions at $r<3$ cm disappeared totally; however, the particle density at $r\sim5$ cm became twice the initial particle density. Similarly, the negative ions at $r<5$ cm disappeared totally after 15 μs; however, the particle densities at 8–10 cm were higher than the initial particle density. Note that the particle density is plotted against r, i.e., in the cylindrical coordinate system in Fig. 9(b). Because the cell volume increases with r, the number density decreases with r even if the same number of particles exist. This effect is clearly shown in Fig. 9(b). Although the density around the central region drastically decreased in several μs, approximately 60% of the test particles are remained even at 5 μs.

Since the negative ion is a minority species, the interactions between them can be neglected. Thus, the relative H^- density profile can be obtained by integrating the particle number density shown in Fig. 9(b) in each time step until all the particles disappear. In Fig. 9(c), the radial cell size for evaluating the H^- density from the simulation is 3 mm. Other parameters such as time step size and test particle number were the same as those used in the calculation performed in Fig. 9(b). In Fig. 9(c), case (ii) represents the H^- density profiles obtained from the particle simulation using 5000 test H^- particles for the degrees of dissociation F of 4%, 6%, and 8%. The calculation revealed a peak at $r\sim5$ cm, and decreased as the radius increased above $r\sim5$ cm; the calculated profile was in agreement with n_-. In the peripheral region, the calculated density decreased with an increase in the degree of dissociation because the collision with H is one of the major H^- extinction processes in the peripheral region. Based on the comparison between the calculation and experimental results, it can be said that the transport of negative ions is one of the key processes to determine the H^- density profiles in magnetized plasmas.

To investigate the sensitivity of the H^- density profile to the electric field strength, the calculations were performed by changing the electric field strength independently. Figure 10 shows the calculated H^- density profile for different electric field strengths under the assumption that the H^- density calculated in Fig. 9(c) for $F=6\%$ is correct at $r\sim6$ cm. Cases (a), (b), and (c) correspond to the results without the electric field, with the experimental electric field, and twice the ex-

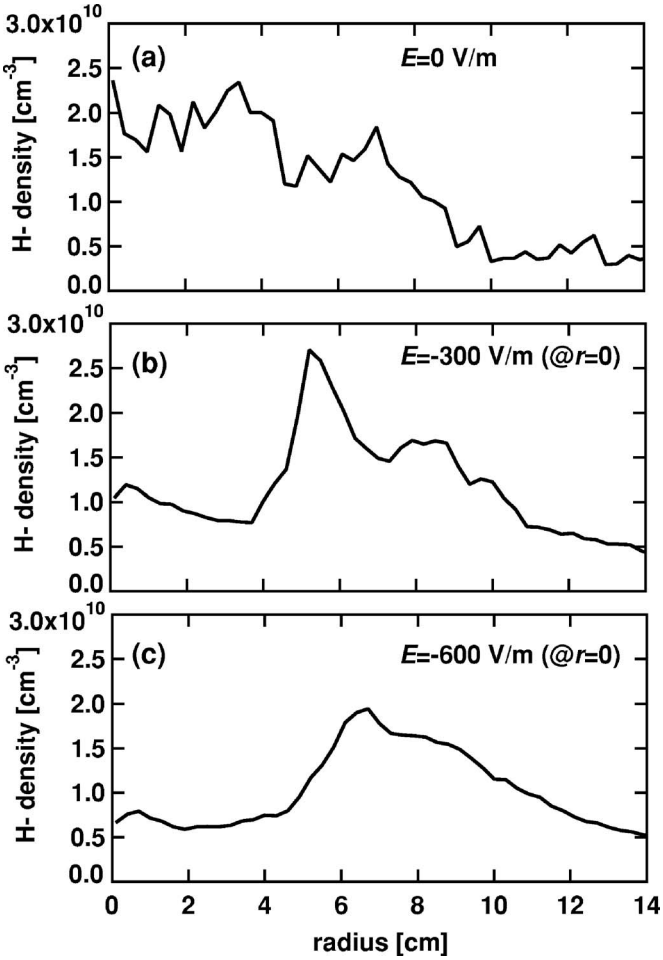

FIG. 10. Negative ion density profile calculated for different electric field strengths: (a) without electric field, (b) with experimental electric field, and (c) twice the experimental electric field strength. The electron density and temperature profiles shown in Fig. 2(a) are used in the calculation.

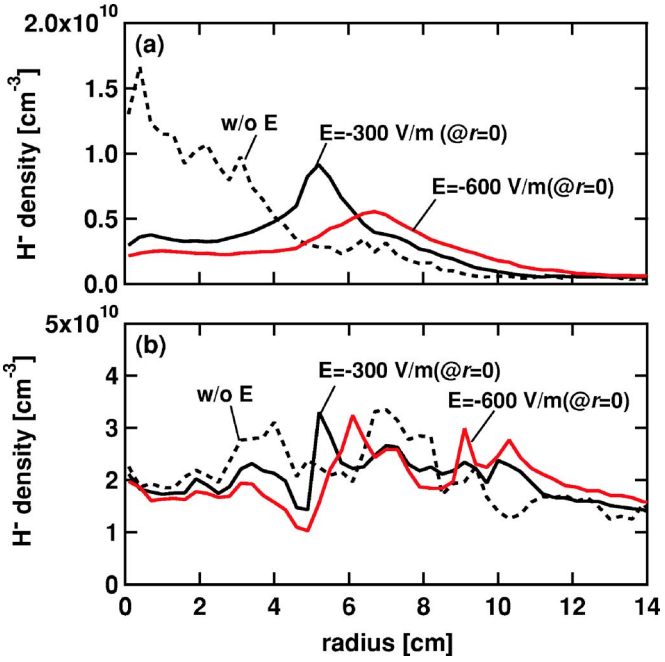

FIG. 11. (Color online) H⁻ density profile calculated under the assumption that n_e becomes (a) one third of and (b) five times that in Fig. 2(a). Three cases corresponding to three different electric field strengths are presented.

perimental electric field strength, respectively. Without the electric field, the H⁻ density profile does not exhibit a clear peak in the peripheral region even if diffusive transport is included. When the electric field is introduced, a clear peak can be observed around $r=5-7$ cm, as shown in Figs. 10(b) and 10(c). It was demonstrated that the electric field plays an important role in the transport of H⁻ under the present experimental conditions.

It is expected that the transport effect is suppressed when the lifetime of H⁻ is shorter than the time necessary for the transport. Figure 11(a) shows the calculated H⁻ density profiles under the assumption that n_e becomes (a) one third of and (b) five times that in the experiment for three different electric field strengths. The number of test H⁻ particles used for the calculations shown in Figs. 11(a) and 11(b) are 5000 and 25000, respectively. In both calculations, the H density is set to be the same as that in Fig. 9, and the parallel transport effect is considered in the simplified model. Although these ambiguities exist when the H⁻ profiles are discussed, it is possible to discuss the sensitivity of the H⁻ density profiles to the electric field strength based on the calculation results. The H⁻ density profile is clearly affected by the electric field, as shown in Fig. 11(a). On the other hand, the effect of the electric field on the H⁻ density profile is insignificant, as shown in Fig. 11(b). When the electron density is high, the lifetime of H⁻ is so short that it is difficult for them to be transported to the peripheral region. When the electron density is low, the extinction due to the electron impact and mutual neutralization becomes insignificant; therefore, the lifetime of H⁻ becomes longer. Consequently, the profile of H⁻ appears to be more sensitive to the electric field strength.

IV. CONCLUSIONS

The behavior of hydrogen negative ions was investigated experimentally and numerically in the divertor simulator MAP-II. To evaluate the negative ion density n_- and its ratio to the electron density n_-/n_e using the laser photodetachment method, the influence of the magnetic field was considered. In particular, by using the ion current and the relative value of the electron current, we deducted the effect of the anomaly of the current voltage characteristic of a probe; such anomalies frequently occur in low-temperature recombining plasmas. Experimentally, it was observed that the negative ions mainly existed in the peripheral region of the plasma column and the maximum density ratio n_-/n_e at $r\sim 10$ cm was approximately 15%.

Since the H⁻ density profile cannot be explained by the rate equation calculation, in which local negative ion production and extinction rates were balanced, we developed a particle simulation code for investigating the effect of the cross-field transport of the negative ions. When the effects of radial transport were considered, the calculated profile of the negative ion density agreed with the experimental results. With the help of the electric field and the elastic collisions, it was

shown that the negative ions can be transported to the radially outer region where the lifetime of negative ions is reasonably long.

In linear discharge devices such as a divertor simulator, two separate regions such as those in negative ion sources are formed naturally. In other words, rovibrationally excited hydrogen molecules are produced in the central region, while the lifetime of the negative ions in the peripheral region is reasonably long. Furthermore, the potential well, which may be produced by the ambipolar diffusion process across the magnetic field, is formed in the plasmas; therefore, the produced negative ions are transported to the peripheral region. This transport effect can enhance the negative ion density in the peripheral region.

ACKNOWLEDGMENTS

The authors thank Professor A. Tonegawa of Tokai University for his valuable comments.

This work was supported in part by a Grant-in-Aid for Scientific Research received by S. Kajita from the Japan Society for the Promotion of Science (JSPS) Research Fellowships for Young Scientists (No. 17-7503), and in part by a NIFS collaborative research program (No. NIFS04K0AB009) directed by S. Kado.

[1] S. Kado, Y. Iida, S. Kajita, D. Yamasaki, A. Okamoto, B. Xiao, T. Shikama, T. Oishi, and S. Tanaka, J. Plasma Fusion Res. **71**, 810 (2005).
[2] J. Wesson, *Tokamaks*, 3rd ed. (Oxford Science, Oxford, 2004), Chaps. 5.5 and 2.14.
[3] I. Krasheninnikov, A. Y. Pigarov, and D. J. Sigmar, Phys. Lett. A **214**, 295 (1996).
[4] A. Kono and K. Kato, Appl. Phys. Lett. **77**, 495 (2000).
[5] M. Bacal, Nucl. Fusion **46**, S250 (2006).
[6] K. N. Leung, K. W. Ehlers, and M. Bacal, Rev. Sci. Instrum. **54**, 56 (1983).
[7] O. Fukumasa and R. Nishida, Nucl. Fusion **46**, S275 (2006).
[8] D. Riz and J. Pamela, Rev. Sci. Instrum. **69**, 914 (1998).
[9] M. Bacal, A. Hatayama, and J. Peters, IEEE Trans. Plasma Sci. **33**, 1845 (2005).
[10] G. P. Lawrence, R. K. Beauchamp, and J. L. McKibben, Nucl. Instrum. Methods **32**, 357 (1965).
[11] J. Uramoto, AIP Conf. Proc. **158**, 319 (1987).
[12] M. Wada, S. Takeshima, H. Tsuda, and M. Sasao, Rev. Sci. Instrum. **61**, 430 (1990).
[13] A. Ando, T. Kuroda, Y. Oka, O. Kaneko, A. Karita, and T. Kawamoto, Rev. Sci. Instrum. **61**, 442 (1990).
[14] Y. Abate and H. J. Ramos, Rev. Sci. Instrum. **71**, 3689 (2000).
[15] K. Jimbo, Phys. Fluids **27**, 2752 (1984).
[16] S. Kajita, S. Kado, N. Uchida, T. Shikama, and S. Tanaka, J. Nucl. Mater. **313-316**, 748 (2003).
[17] S. Kado, S. Kajita, D. Yamasaki, Y. Iida, B. Xiao, T. Shikama, T. Oishi, A. Okamoto, and S. Tanaka, J. Nucl. Mater. **337-339**, 166 (2005).
[18] A. Tonegawa, M. Ono, Y. Morihira, H. Ogawa, T. Shibuya, K. Kawamura, and K. Takayama, J. Nucl. Mater. **313-316**, 1046 (2003).
[19] M. Ono, A. Tonegawa, K. Kumita, T. Shibuya, and K. Kawamura, J. Nucl. Mater. **337-339**, 261 (2005).
[20] M. Bacal, Rev. Sci. Instrum. **71**, 3981 (2000).
[21] A. Tonegawa, K. Kumita, M. Ono, T. Shibuya, and K. Kawamura, Jpn. J. Appl. Phys., Part 1 **45**, 8212 (2006).
[22] A. Matsubara, A. Tonegawa, T. Shibuya, K. Sato, K. Kawamura, and K. Takayama, J. Appl. Phys. **89**, 5326 (2001).
[23] S. Kado, S. Kajita, T. Shikama, Y. Iida, D. Yamasaki, A. Okamoto, and S. Tanaka, Contrib. Plasma Phys. **46**, 367 (2006).
[24] S. Kajita, D. Nishijima, N. Ohno, and S. Takamura, J. Appl. Phys. **100**, 103304 (2006).
[25] S. Kajita, S. Kado, T. Shikama, B. Xiao, and S. Tanaka, Contrib. Plasma Phys. **44**, 607 (2004).
[26] S. Kajita, S. Kado, A. Okamoto, and S. Tanaka, Jpn. J. Appl. Phys., Part 1 **44**, 8661 (2005).
[27] S. Kajita, S. Kado, and S. Tanaka, Plasma Sources Sci. Technol. **14**, 566 (2005).
[28] S. Kajita, S. Kado, A. Okamoto, and S. Tanaka, Phys. Rev. E **70**, 066403 (2004).
[29] M. Bacal, A. Bruneteau, and M. Nachman, J. Phys. (Paris), Lett. **42**, L5 (1981).
[30] S. Kajita, S. Kado, and S. Tanaka, Contrib. Plasma Phys. **46**, 373 (2006).
[31] N. Ezumi, N. Ohno, K. Aoki, D. Nishijima, and S. Takamura, Contrib. Plasma Phys. **38**, S31 (1998).
[32] N. Ohno, N. Tanaka, N. Ezumi, D. Nishijima, and S. Takamura, Contrib. Plasma Phys. **41**, 473 (2001).
[33] P. C. Stangeby, *The Plasma Boundary of Magnetic Fusion Devices* (Institute of Physics, Bristol, 2001).
[34] R. D. Monk, A. Loarte, A. Chankin, S. Clement, S. J. Davies, J. K. Ehrenberg, H. Y. Guo, J. Lingertat, G. F. Matthews, M. F. Stamp, and P. C. Stangeby, J. Nucl. Mater. **241-243**, 396 (1997).
[35] S. Kado, H. Kobayashi, T. Oishi, and S. Tanaka, J. Nucl. Mater. **313-316**, 754 (2003).
[36] N. S. J. Braithwaite and J. E. Allen, J. Phys. D **21**, 1733 (1988).
[37] A. G. Nikitin, F. E. Balghiti, and M. Bacal, Plasma Sources Sci. Technol. **5**, 37 (1996).
[38] F. E. Balghiti-Sube, F. G. Baksht, and M. Bacal, Rev. Sci. Instrum. **67**, 2221 (1996).
[39] M. Nishiura, M. Sasao, and M. Bacal, J. Appl. Phys. **83**, 2944 (1998).
[40] H. Naitou, Y. Sakurai, Y. Tauchi, O. Fukumasa, M. Yagi, Y. Yamagata, K. Uchino, and K. Muraoka, Plasma Phys. Controlled Fusion **46**, 1217 (2004).
[41] R. J. Goldston and P. H. Rutherford, *Introduction to Plasma Physics* (Institute of Physics, Philadelphia, 1995), Chaps. 10 and 11.
[42] M. Kojima and S. Takamura, J. Nucl. Mater. **220-222**, 1107 (1995).
[43] M. Ohnishi, N. Ao, and J. Wakabayashi, Nucl. Fusion **18**, 856 (1978).
[44] R. Janev, W. Langer, K. Evans, and D. E. Post, *Elementary Processes in Hydrogen-Helium Plasmas* (Springer, Berlin, 1987), p. 230.
[45] M. S. Huq, L. D. Doverspike, and R. L. Champion, Phys. Rev. A **27**, 2831 (1983).
[46] J. Wadehra, Phys. Rev. A **29**, 106 (1983).
[47] B. Xiao, S. Kado, S. Kajita, and D. Yamasaki, Plasma Phys. Controlled Fusion **46**, 653 (2004).
[48] B. Xiao, S. Kado, S. Kajita, D. Yamasaki, and S. Tanaka, J. Nucl. Mater. **337-339**, 1082 (2005).